

PREPARED FOR SUBMISSION TO JCAP

Making maps of cosmological parameters

Suvodip Mukherjee,^{a,b,c} and Benjamin D. Wandelt^{a,b,c,d}

^aInstitut d'Astrophysique de Paris (IAP), UMR 7095, CNRS/UPMC Université Paris 6, Sorbonne Universités, 98 bis boulevard Arago, F-75014 Paris, France

^bInstitut Lagrange de Paris (ILP), Sorbonne Universités, 98 bis Boulevard Arago, 75014 Paris, France

^cCenter for Computational Astrophysics, Flatiron Institute, 162 5th Avenue, 10010, New York, NY, USA

^dDepartments of Physics and Astronomy, University of Illinois at Urbana-Champaign, 1002 W Green St, Urbana, IL 61801, USA

E-mail: smukherjee@flatironinstitute.org, wandelt@iap.fr

Abstract. We provide a fast algorithm to diagnose any directional dependence in the cosmological parameters by calculating maps of local cosmological parameter estimates and their joint errors. The technique implements a fast quadratic estimator technique based on Wiener filtering and convolution of the sky with a patch shape. It uses only three map-resolution spherical harmonic transforms per parameter and applies to any data set with full sky or a partial sky coverage. We apply this method to Planck SMICA-2015 and obtain fluctuation map for six cosmological parameters. Our estimate shows that the Planck data is consistent with a single global value of the cosmological parameters and is not influenced by any severe local contaminations. This method is applicable also to other angular or 3D data sets of future missions to scrutinize any local variation in the cosmological parameters.

Contents

1	Introduction	1
2	How to map cosmological parameter variations	2
2.1	Formalism for arbitrary parameter patches	2
2.2	Azimuthally symmetric patches	5
2.3	Nature of the approximation	6
2.4	Implementation on CMB simulations	7
2.5	Computational cost	9
3	Implementation on Planck SMICA map of CMB	10
3.1	Procedure	10
3.2	Parameter variation in Planck SMICA map	11
3.3	Comparison of Planck SMICA results with CMB simulations	15
4	Conclusions	16

1 Introduction

The successful history of several cosmological missions in CMB [1–13] have paved the path of precision cosmology and several upcoming missions like EUCLID [14], LSST [15], SKA [16], PIXIE [17] and LiteBIRD [18] have the potential to vastly enhance the precision with which we know the cosmological parameters. With increasing signal-to-noise, and more complex inference tasks, systematics will become the primary challenge to cosmological parameter inference. The accurate estimation of cosmological parameters from these next generation missions require advanced methods and sophisticated techniques to accurately remove systematic errors and non-cosmological contaminations from the observed data.

Inferring parameters from a cosmological data set requires a great deal of care. The approach is typically Bayesian where selection of robust features of the data, detailed statistical modelling of the signal, the systematics, and the measurement process leads to a likelihood that is combined with carefully chosen priors. The resulting posterior probability density for the parameters is then usually explored by sampling it with Markov Chain Monte Carlo (MCMC) [19]. Standard analyses assume statistical homogeneity and isotropy of the universe, a natural assumption since there is no strong evidence for violations of these symmetries. However, the presence of systematics like foreground contamination, anisotropic noise and beam, and other perhaps incompletely modelled instrumental, environmental or astrophysical systematics, may introduce biases in the parameters. These systematics would not be expected to respect the rotational or translational symmetries of an isotropic and homogenous universe. So a diagnostic that estimates parameters on many sky patches and visualises the way these estimates vary

across the sky, that is a *parameter map*, would be a useful tool to test for the presence of systematics and to obtain clues as to their origin.

In addition, in the absence of strong systematics such an analysis has the potential to reveal a first hint of violations of the isotropy or homogeneity assumptions. Even in a globally symmetric universe, our sky could contain statistical anisotropy of cosmological origin. For examples, physical parameters could take different values in different domains and we might sit between two or more such domains. This approach was taken in [20–22] to test for direction dependence of the cosmological parameters from Supernovae data. Any such hints could be followed up with dedicated searches, testing specific physical models that would predict such variations [23–31]. The presence of enhanced temperature fluctuations in the local patches of the sky is also of interest due to predictions from theoretically motivated models and were studied in past using WMAP data [32–38].

MCMC samplers are now the standard approach to cosmological parameter inference. But to run an MCMC chain in each patch to infer the cosmological parameters is expensive. In this paper, we devise a fast, efficient and simple algorithm to estimate directional dependence of cosmological parameters and implement it on CMB maps. We show that the cosmological parameters can be computed through a quadratic estimator that implicitly projects a local deviation of the angular power spectrum of the signal onto a parameter change from a fiducial value. The appropriate projection is done by applying an optimal filter. Optimal or Wiener filtering is a powerful method that is widely used in cosmology data analysis in several contexts [39–52].

The variation in the angular power spectrum of the CMB temperature field can be related to leading order to the variation in cosmological parameters by performing a Taylor series expansion. Our method shares this feature with the method described in [53] but goes beyond it by showing how to do parameter analysis on many patches without having to compute the power spectra explicitly for the cost of a very mild approximation. The result is a map of parameter estimates and correlated uncertainties. Owing to its computational simplicity this method can be implemented on large data sets even with complicated sky coverage efficiently and with limited computational cost.

The paper is organized as follows. In Sec. 2, we lay out the basic formalism of this method. In Sec. 3.1, we discuss the implementation of this method on CMB temperature maps. We obtain the map for variation of cosmological parameters from the publicly available Planck SMICA map [54] and compare it with a simulated CMB map in Sec. 3. We summarize and conclude in Sec. 4.

2 How to map cosmological parameter variations

2.1 Formalism for arbitrary parameter patches

To achieve our goal of developing a fast diagnostic to explore the data we will want to perform parameter analyses on many patches of the data. Each patch will necessarily provide a weaker constraint on the parameters than the full data set. As a consequence we will content ourselves with an asymptotic approach, that returns a parameter estimate for each patch, together with an asymptotic error estimate, as follows.

We develop the method for the example of the cosmic microwave background temperature (CMB) fluctuations on the sphere but applies without change to any other scalar field on the sphere. Fields on rectangular domains can be treated strictly analogously by replacing spherical harmonics with Fourier coefficients. The discussion can also be generalized to spin- n fields, such as CMB polarization anisotropies or lensing shear measurements without difficulty.

The CMB data map containing the measured temperature and polarization anisotropies $d(\hat{n})$ can be expressed in the spherical harmonic basis as

$$d(\hat{n}) = \sum d_{lm} Y_{lm}(\hat{n}), \quad (2.1)$$

where d_{lm} have zero mean, are mutually uncorrelated and have variance C_l , the power spectrum. For full sky, noise-free data the optimal estimate of the C_l is

$$\hat{C}_l = \frac{\sum_m d_{lm} d_{lm}^*}{2l+1}, \quad l = 2, \dots, L, \quad (2.2)$$

which can be written using \mathbf{P}_l , the operator projecting onto angular wavenumber l

$$\hat{C}_l = \frac{1}{2l+1} \mathbf{d}^T \mathbf{P}_l \mathbf{d}. \quad (2.3)$$

For the estimation of the cosmological parameters in different patches of the sky, each patch will be defined by the patch shape window $W^p(\hat{n}_j)$,

$$W^p(\hat{n}_j) = \begin{cases} 1 & \text{if pixel } j \text{ is in patch } i, \\ 0 & \text{otherwise} \end{cases} \quad (2.4)$$

for the case of a sharp-edged, unapodized patch window. It will be convenient to define the operator \mathbf{W}^p as the diagonal matrix with elements $W_{jj}^p = W^p(\hat{n}_j)$ such that the map of temperature fluctuations in patch i is $\mathbf{W}^p \mathbf{d}$. The pseudo power spectrum on this patch \tilde{C}_l^p [55, 56] is defined as

$$\tilde{C}_l^p = \frac{1}{2l+1} (\mathbf{W}^p \mathbf{d})^T \mathbf{P}_l \mathbf{W}^p \mathbf{d}, \quad (2.5)$$

provides a statistical summary of the information the patch i contains about the cosmological parameters¹. In expectation, this is related to the full sky power spectrum C_l by the mode coupling matrix $M_{ll'}^p$ imposed by the patch shape and the noise bias N_l^p

$$\langle \tilde{C}_l^p \rangle = \sum_{l'} M_{ll'}^p \langle C_{l'} \rangle + N_l^p. \quad (2.6)$$

We have omitted the instrumental transfer function and the beam for clarity of presentation; those can be included in the usual way, as shown in [57].

¹In fact, any power spectrum estimate may be used. In the faster, harmonic-space variant of our method described section 2.2 we specialize to a pseudo-spectrum estimator to achieve a drastic reduction in computational cost. The well-known pseudo-spectrum is a member of this class.

For a fiducial set of n_θ cosmological parameters θ_j^{fid} , $j = 1, \dots, n_\theta$, let the predicted global CMB power spectrum be $C_l^{\text{fid}} \equiv C_l(\theta^{\text{fid}})$. As the cosmological parameters determine the power spectrum of the CMB, any patch-dependence of the cosmological parameters translates into a patch-dependence of the power spectrum. Defining θ_j^p to be the cosmological parameters in patch p , the deviation in the value of the measured spectrum \tilde{C}_l^p from that expected in the fiducial model can be written as

$$\delta\tilde{C}_l^p = \tilde{C}_l^p - \tilde{C}_l^{\text{fid } p} - N_l^p, \text{ where } \tilde{C}_l^{\text{fid } p} = \sum_{l'} M_{ll'}^p C_{l'}^{\text{fid}}. \quad (2.7)$$

The $\delta\tilde{C}_l^p$ capture any deviation of the power spectrum in patch p from that which is expected given the fiducial, global model and the mode-coupling induced by the patch shape.

Writing up to linear order in the parameter variation, we have

$$\delta\tilde{C}_l^p = \sum_j^{n_\theta} \left. \frac{\partial \tilde{C}_l^{\text{fid } p}}{\partial \theta_j} \right|_{\theta_j = \theta_j^{\text{fid}}} (\theta_j^p - \theta_j^{\text{fid}}) + \dots \quad (2.8)$$

In the following, we switch to matrix notation. We write an $(L-1)$ -vector $\delta\mathbf{c}^p$ for the quantity in Eq. 2.7 and collect the derivatives into the $(L-1) \times n_\theta$ -matrix \mathbf{D}^p . The parameters are the n_θ -vector $\boldsymbol{\theta}^p$. Then Eq. (2.8) becomes

$$\delta\mathbf{c}^p = \mathbf{D} \left(\boldsymbol{\theta}^p - \boldsymbol{\theta}^{\text{fid}} \right) = \mathbf{D}^p \delta\boldsymbol{\theta}^p, \quad (2.9)$$

where the last equality defines $\delta\boldsymbol{\theta}^p$ which captures the variation from fiducial values of the cosmological parameters in the patch of the sky with the center of the direction given by \hat{n}_i .

The measurement covariance matrix for the power spectrum in a given patch \hat{n}_i is $\mathbf{K}_{\delta\mathbf{c}}^p$, with components $K_{\delta\mathbf{c}}^p = \langle (\delta\tilde{C}_l)(\delta\tilde{C}_{l'})^t \rangle$. With these ingredients we can now compute an asymptotically optimal estimator for the $\delta\boldsymbol{\theta}$ in terms of the $\delta\mathbf{c}$ in each patch as follows.

Working in the asymptotic regime where the likelihood for \mathbf{c} is Gaussian to a good approximation, the maximum likelihood estimate for the parameter deviation in each patch is

$$\hat{\delta\boldsymbol{\theta}}^p = (\mathbf{F}^p)^{-1} \mathbf{D}^{p T} (\mathbf{K}_{\delta\mathbf{c}}^p)^{-1} \delta\mathbf{c}^p, \quad (2.10)$$

with covariance

$$\mathbf{K}_{\boldsymbol{\theta}}^p = \langle \delta\hat{\boldsymbol{\theta}}^p \delta\hat{\boldsymbol{\theta}}^{p T} \rangle = (\mathbf{F}^p)^{-1}, \quad (2.11)$$

where \mathbf{F}^p is the Fisher matrix in patch p (see [58] for a discussion of the Fisher matrix). In the asymptotic case we are considering here

$$F_{ij} = \mathbf{D}^T \mathbf{K}_{\delta\mathbf{c}}^{-1} \mathbf{D}. \quad (2.12)$$

Note that given the data vector \mathbf{c} , the parameter estimate $\hat{\boldsymbol{\theta}} = \boldsymbol{\theta}^{\text{fid}} + \delta\hat{\boldsymbol{\theta}}$ saturates the Cramer Rao bound; the parameter estimates are optimal. This result is analogous

to the result of [53] which focuses on compressing the data to derive a Fisher-optimal likelihood for MCMC exploration. Our estimate comes from the direct maximization (without running an MCMC chain) of the same, optimal likelihood for every patch.

The method as described so far applies under quite general circumstances such as when the individual patches have very different shapes or noise properties. Since the method does not require running MCMC chains it is fast enough to run an analysis on 48 sky patches from the Planck data in about one hour on a standard laptop. The parameter estimates in different patches can be computed efficiently in parallel. We will discuss additional computational considerations in subsection 2.5.

We will now turn to a harmonic space technique that accelerates computing the parameter maps under some additional assumptions.

2.2 Azimuthally symmetric patches

Assume that we choose the patches as (possibly apodized) circular disks centered on all pixels of a parameter map². All patches have identical size, shape, and radial profile. The patch window is then a function of the angular distance to the patch center \hat{n}_p only,

$$W^p(\hat{n}_i) \equiv W(\hat{n}_p, \hat{n}_i) = \sum_l \frac{2l+1}{4\pi} W_l P_l(\hat{n}_p \cdot \hat{n}_i). \quad (2.13)$$

As a consequence, the coupling matrix $M_{ll'}$, the \hat{C}_l^{fid} , and the \mathbf{D} , are the same for all patches. If the beam, instrumental transfer function and power spectrum co-variance can also be approximated as the same for all patches we can use the following harmonic-space method.³ We will drop the explicit patch superscript for quantities that are the same for all patches.

Let us compute the parameters for one such circular patch. From Eq. 2.10 we find that

$$\delta \hat{\boldsymbol{\theta}}^p = \mathbf{F}^{-1} \mathbf{D}^T \mathbf{K}_{\delta \mathbf{c}}^{-1} \delta \mathbf{c}^p, \quad (2.14)$$

We can define the rectangular $(n_\theta \times L)$ -matrix with elements

$$O_l^j \equiv \sum_{k,l'} F_{jk}^{-1} D_{kl'}^T K_{\delta \mathbf{c} l' l}^{-1} \frac{1}{2l+1}, \quad (2.15)$$

²Any other azimuthally symmetric patch shapes, such as annuli can be treated without modification of the formalism.

³These assumptions will break down for patches that intersect the survey mask. For quick analysis, these edge cases might simply be ignored. If desired, they can be treated separately by the method described in the previous subsection. Pixels masked to exclude bright point sources will occur all over the map, but the coupling matrix $M_{ll'}$ only depends on the average number of these exclusions per steradian and may therefore be treated as constant across the sky to a good approximation. If the noise power varies significantly across the sky, the resulting noise bias in the parameters can be corrected for simply by subtracting the effect on parameters of the noise bias term in Eq. 2.6 by computing the average parameter map on signal-free noise simulations. We ignore the variation this would induce for the covariances of the parameter estimates, which could again be estimated with a modest number of Monte Carlo simulations.

Considering each of the n_θ rows separately, each element of $\delta\hat{\boldsymbol{\theta}}$ in equation 2.10 can be computed simultaneously for all pixels in the parameter map, as follows.

We want to extract from the map the portion whose fluctuations compress the information about cosmological parameters. The parameter components of equation 2.14 can be rewritten as

$$\delta\hat{\theta}_j^p = \sum_l O_{jl} \left[(\mathbf{W}^p \mathbf{d})^T \mathbf{P}^l \mathbf{W}^p \mathbf{d} - (\tilde{C}_l^{\text{fid}} + N_l) \right], \quad (2.16)$$

$$= (\mathbf{W}^p \mathbf{d})^T \mathbf{O}^j \mathbf{W}^p \mathbf{d} - b_j^p, \quad (2.17)$$

where we defined $\mathbf{O}^j \equiv \sum_l O_l^j \mathbf{P}^l$ and b_j^p is the sum of the expected isotropic signal and noise contribution to the parameter estimate in the patch.

Aside from reducing the number of pre-computations due to the simplified setup this expression is no faster to evaluate than Eq. 2.14. But approximating this expression by reversing the order of the operators \mathbf{O}^j and \mathbf{W}^p in the first term of 2.17 results in

$$(\mathbf{W}^p \mathbf{d})^T \mathbf{O}^j \mathbf{W}^p \mathbf{d} \approx (\mathbf{W}^p \mathbf{d})^T \mathbf{W}^p \mathbf{O}^j \mathbf{d} = \sum_i W_i^p{}^2 d_i [\mathbf{O}^j \mathbf{d}]_i, \quad (2.18)$$

the dot product of the patch window with the quadratic map obtained by the pixelwise multiplication of the filtered data map with its unfiltered version. The parameters in *all* patches can therefore be obtained using the following series of operations: 1) Transform the data map into harmonic space; 2) Generate n_θ maps by multiplying with each \mathbf{O}^j and transforming back to pixel space; 3) Multiply every pixel of this map by the corresponding pixel in the data map; 4) Then convolve each of the resulting maps with the square of the patch window in harmonic space to produce the parameter maps at the desired resolution. This last step can be done efficiently in harmonic space, and the final transform to pixel space needs only to be done at the coarser patch resolution (rather than the full pixel resolution) to produce the parameter map.

In total this requires $1 + 3n_\theta$ harmonic transforms covering the full bandwidth and resolution of the data map, and then another n_θ low-bandwidth and low-resolution transforms to produce the parameter maps on a coarse pixelisation. The full resolution transforms dominate the scaling in the relevant regime and give $O\left((1 + 3n_\theta)n_{\text{pix}}^{3/2}\right)$. Contrast this with the n_{patch} full transforms to produce the $\delta\mathbf{c}^p$ and the transforms required to compute the coupling matrices that dominate the $O\left(2n_{\text{patch}}n_{\text{pix}}^{3/2}\right)$ computational cost Eq. 2.14. We will compare the computational aspects of the two methods in more detail in section 2.5.

2.3 Nature of the approximation

The map obtained by using Eq. 2.18 differs slightly from the one defined in Eq. 2.17, even for azimuthally symmetric patches. The difference comes from the way the patch window is applied. By design, only pixels within the patch p affect the parameter estimate for that patch in Eq. 2.17. The estimates from Eq. 2.18 however result from the application

of the optimal filters \mathbf{O}^j to the entire sky map (after masking of foreground contaminated regions) and then measuring the variance within sky patch p .

Since the real-space convolution kernels corresponding to the \mathbf{O}^j have finite support parameter estimates in neighbouring patches will be more strongly correlated than would be the case in the original approach Eq. 2.17; on the other hand the parameter estimates would be less noisy, since acting with the kernels on the full sky would allow a cleaner separation of the contributions each parameter makes to the variance in the patch.

Radially truncating the pixel-space kernels corresponding to the \mathbf{O}^j would improve the approximation to affect only immediately adjacent patches. This can be done simply by Legendre transforming the rows of O_l^j , truncating at the cosine of angular radius of the patch kernel and transforming back. This recovers the same $d_i[\mathbf{O}^j d]_i$ for pixels in the center of the patch but would still couple the edge of this map to pixels in neighbouring patches. We find the effect of the approximation to be modest in our numerical tests, and did therefore not implement the kernel truncation in any of the applications presented in this paper.

2.4 Implementation on CMB simulations

The azimuthal symmetry method and the arbitrary mask method mentioned in Eq. (2.17) and Eq.(2.10)) respectively are now implemented for an ideal simulated map of a fixed realization. We implemented these methods on the simulated CMB map obtained by HEALPix [59] using the best-fit Planck cosmological parameters [60], to get a fluctuation map for six cosmological parameters ($A_s, n_s, O_b h^2, O_c h^2, H_0, A_L$). We applied Eq. (2.17) and Eq.(2.10)) with a symmetric circular patch of radius 16.5° and obtained the parameter maps as depicted in Fig. 1 and Fig. 2 respectively for both these cases. As expected from a simulated sky, all the fluctuations in the cosmological parameters are consistent with the best-fit value used in the analysis. We also obtain a cosmological parameter map in high resolution using azimuthally symmetric method. A relative RMS difference in the values from both these methods are less than 1 sigma and are shown in Table 1. This indicates that both the method are accurate and giving us consistent results. The azimuthally symmetric method is significantly computationally faster than the other method. The details on the computational cost are discussed in the Sec. 2.5.

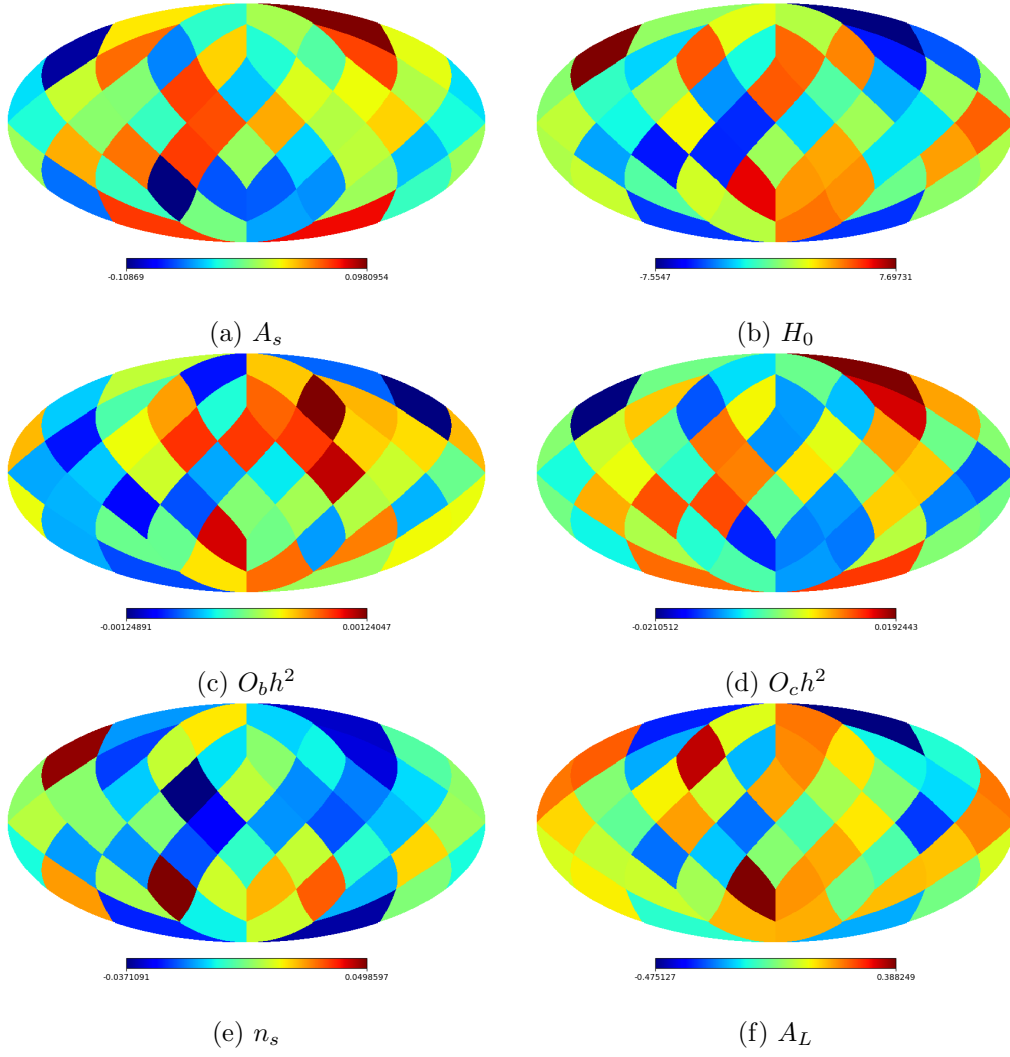


Figure 1: The azimuthally symmetric method mentioned in Eq. 2.17 is implemented on simulated CMB sky to obtain six cosmological parameter maps for a patch radius of 16.5° .

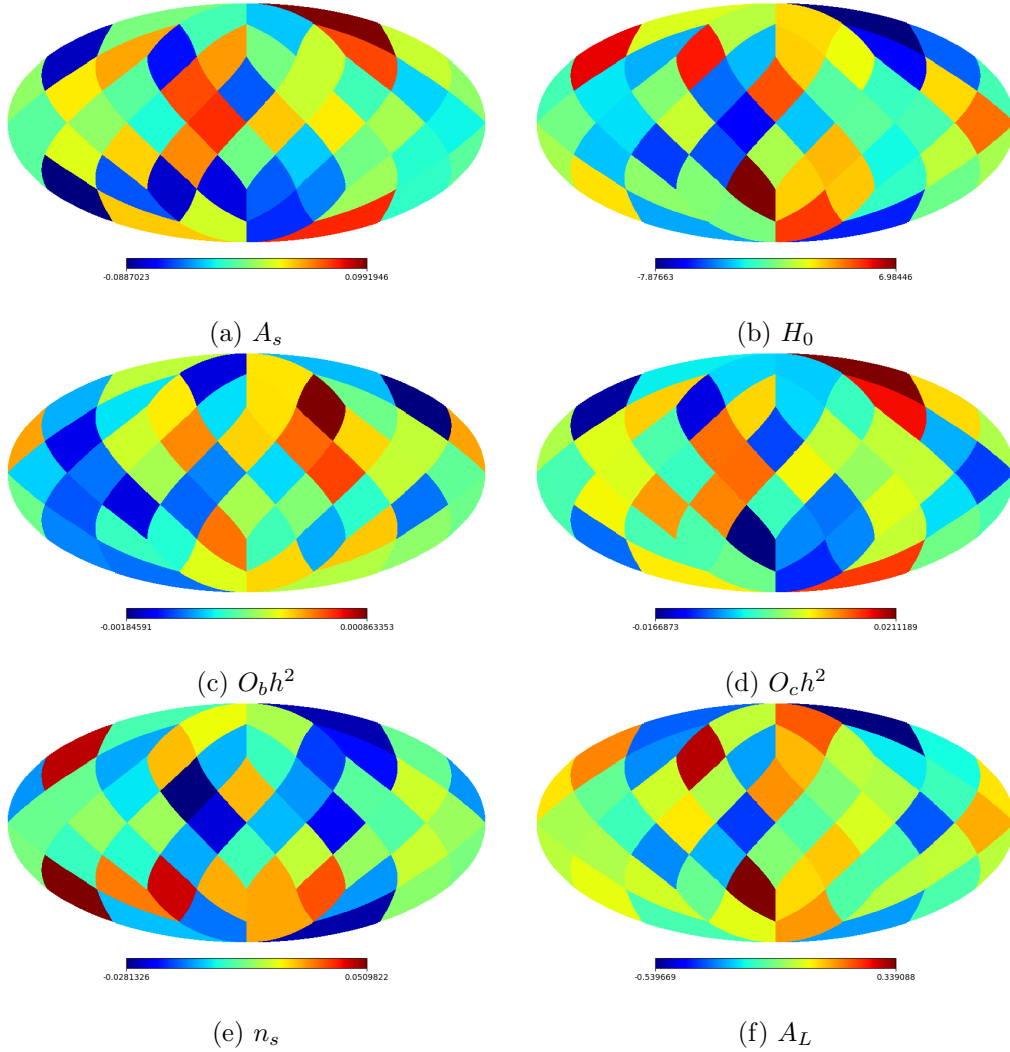


Figure 2: The arbitrary mask case, Eq. 2.10 implemented on the same simulated CMB sky as in Fig. 1 to obtain six cosmological parameter maps for a patch radius of 16.5° . Note that while the approximation in Eq. (2.18) produces minor changes, the binning of $\Delta l = 20$ used in the arbitrary patch analysis means the maps are not expected to match exactly.

2.5 Computational cost

Arbitrary patches : For the general case, Eq. 2.10, the computational cost is dominated by the spherical harmonic transforms to compute the pseudo-spectra and coupling matrices for all patches, ie 2 per patch. These computations can be done in parallel for all patches, enabling embarrassingly parallel computation on n_{patch} nodes (in addition to any parallelization of the harmonic transforms). The total number of operations is

Table 1: Root mean square differences between the arbitrary patch and the symmetric patch methods in units of the standard deviation. Note that while the approximation in Eq. (2.18) produces minor changes, the binning of $\Delta l = 20$ used in the arbitrary patch analysis means the results are not expected to agree exactly.

Cosmological Parameters	RMS fluctuations (in units of the standard deviation)
A_s	0.33
H_0	0.26
$O_b h^2$	0.76
$O_c h^2$	0.26
n_s	0.53
A_L	0.28

more than the symmetric case. For the example shown in Fig. 2 the method takes 83 minutes on a 3.5 GHz CPU for the six cosmological parameter maps.

Azimuthally symmetric patches : In this case, we need to perform one transformation for the mask, three spherical harmonic transformations for each parameter at the native resolution of the map and on final transformation to the patch resolution. So, for a set of n_θ parameters, we need to perform $3n_\theta + 1$ high resolution transformations. As a result, for a set of six cosmological parameters, we need to perform 19 high resolution transformations. For a parallel computational process, we can distribute the job to n_θ computers and each computer needs to perform 3 high resolution transformations and one low resolution one. For larger resolution of the parameter map, and hence smaller and more numerous patches, this method rapidly becomes much faster general patch shape. Even for the example shown in Fig. 1 with only 48 parameter patches the method takes 10 minutes on a 3.5 GHz CPU for all six full-sky cosmological parameter maps, a speed-up of a factor of 8.

3 Implementation on Planck SMICA map of CMB

3.1 Procedure

The implementation of the method formulated in Sec. 2 requires calculating three essential ingredients: the covariance matrix for the angular power spectra ($\mathbf{K}_{\delta\mathbf{C}}$), the derivative matrix \mathbf{D} and the estimate of the difference in the angular power spectra of each patches from the fiducial value of the angular power spectra \mathbf{c} .

Calculation of \mathbf{c} : On the $n_{\text{side}} = 2048$ resolution maps of Planck, we applied the Planck SMICA confidence mask as depicted in Fig. 3. We divide the sky into a low resolution $N_{\text{SIDE}} = 2$ map having 48 patches. We then obtain the angular power spectrum C_l from each of these patches using HEALPix [59]. The C_l from the masked sky for each of the patches are corrected using MASTER [57] to take care of the effects of the

partial sky. Then the difference between the estimated $C_l(\hat{n})$ from each patch centered in the direction (\hat{n}) and the fiducial C_l are obtained for each patch. The fiducial C_l is obtained using CAMB [61] by using the fiducial cosmological parameters from Planck [60].

Calculation of $K_{\delta C}$: The binned spectra are taken to have covariance [57]

$$K_{\delta C} = \frac{2}{(2l+1)\Delta l f_{sky}} (C_l + N_l)^2, \quad (3.1)$$

where N_l is the instrumental noise in the SMICA map. The f_{sky} for each patch is different due to different contributions from the galactic mask. The error bar for each patch is therefore different, most notably along the galactic plane where patches have a smaller sky fraction and hence bigger error bars in comparison to the patches at higher latitudes.

Calculation of D : The D matrix captures the derivative of the angular power spectra evaluated at the fiducial value of the parameters C_l . We evaluate the angular power spectra C_l from CAMB [61] by varying each parameter individually and keeping all other parameters fixed at the fiducial cosmological parameters from Planck-2015 [60]. We then obtain the numerical derivative of the angular power spectra at every values of l , and construct a $n_\theta \times l$ dimension matrix, where n_θ indicates the number of parameters.

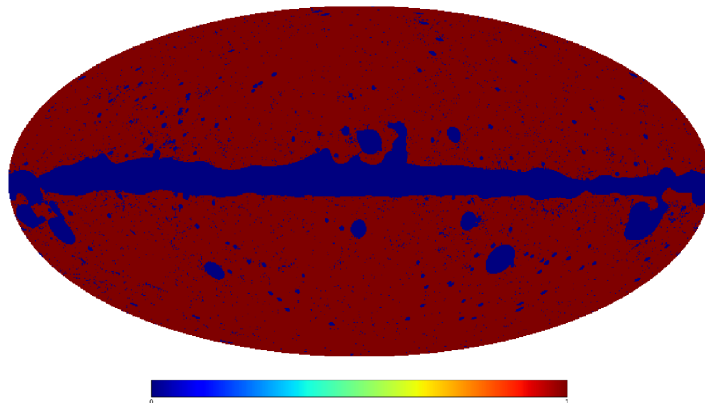


Figure 3: SMICA mask used in the analysis to obtain the variation in the cosmological parameters.

3.2 Parameter variation in Planck SMICA map

Using all the tools mentioned in the previous section, we obtain the variation of cosmological parameters in the sky for six cosmological parameters (A_s , n_s , $O_b h^2$, $O_c h^2$, H_0 , and A_L) for two different choices of $\Delta l = 20$ & 50 . The value of all other parameters are kept fixed at the fiducial Planck best-fit values [60] with $\tau = 0.058$ [62]. The results

of parameter variation are depicted in Fig. 4 and Fig. 5 for $\Delta l = 50$ and 20 respectively. These results show the deviation from the Planck fiducial values. We also overplot the galactic mask on the recovered parameters map to show the contribution of the galactic mask in each patch. The largest deviation is observed for certain patches in the galactic plane, which is anyway not robust for cosmological parameters and not used in the Planck likelihood. The parameters at high latitudes show negligible variation from the fiducial parameter values. To indicate the deviations more clearly, we make histogram plots in Fig. 6 for the deviation of the parameters, inverse weighted with the square-root of the corresponding diagonal element of the inverse of the Fisher matrix for each patch. The histogram plots for the cosmological parameters are obtained for all the patches except the patches in the galactic plane that have sky fraction of less than 1.7 %. The plots indicate that there is no significant deviation in any of the patches and fluctuations from the fiducial parameters in most of the patches are less than 1σ , ie underdispersed compared to expectations. This underdispersion arises because the estimators are correlated between patches. Even though they are calculated from different patches, they share the same realisation of the underlying CMB signal.

To quantify the total patch-to-patch variation in cosmological parameters, we estimate the reduced chi-square defined as

$$\chi(\hat{n}) = \sqrt{\frac{\sum_{ij} \theta_i(\hat{n}) F_{ij} \theta_j(\hat{n})}{\text{Number of parameters}}}. \quad (3.2)$$

This quantity captures the total deviation in the parameter values and is depicted in Fig. 7. It clearly indicates that the Planck SMICA map at high galactic latitude is consistent with the global value of the parameters derived from the Planck likelihood [60]. This map captures the complete SNR of the deviation observed over all the parameters considered here. This extreme variation in a few patches is evident only for the case shown in Fig. 7a, which considers a wide multipole range (20-1300) and reduces significantly for the estimation which considers a lower multipole range (20-520) as shown in Fig. 7b.

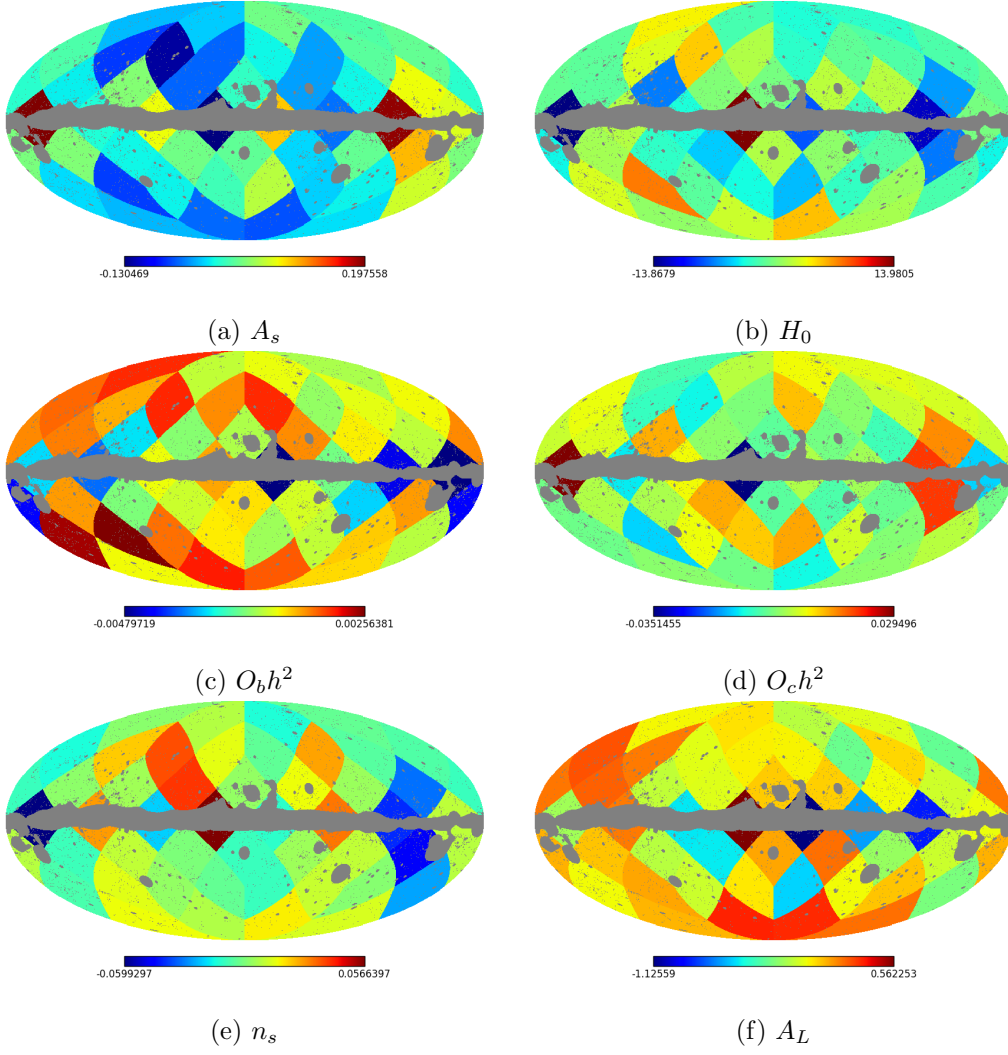


Figure 4: The spatial variation of six cosmological parameters from the Planck SMICA HM1 \times HM2 map are depicted along with the galactic mask used in the analysis. These results are obtained for the bin size of $\Delta l = 50$ using CMB multipoles $[50, 1300]$.

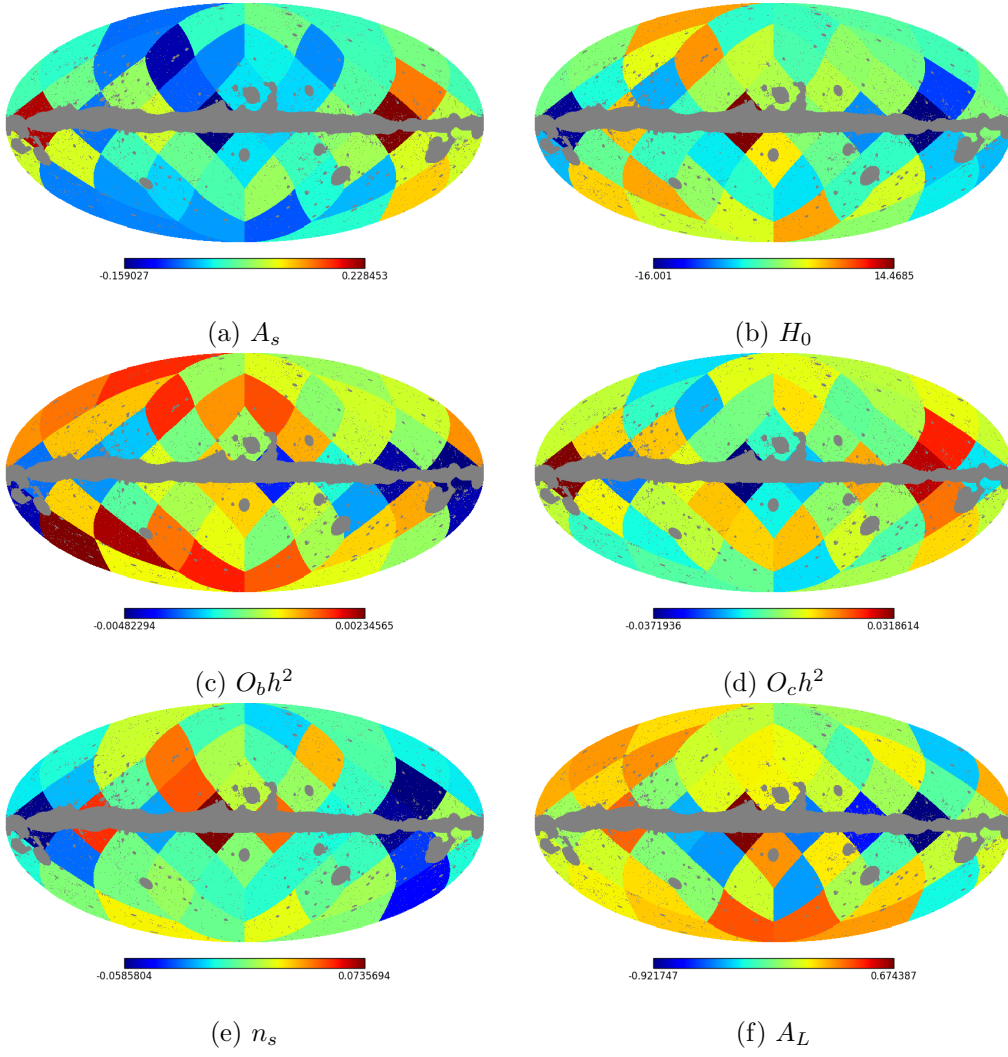


Figure 5: The spatial variation of six cosmological parameters from the Planck SMICA HM1 \times HM2 map are depicted along with the galactic mask used in the analysis. These results are obtained for the bin size of $\Delta l = 20$ using CMB multipoles $[20, 1300]$.

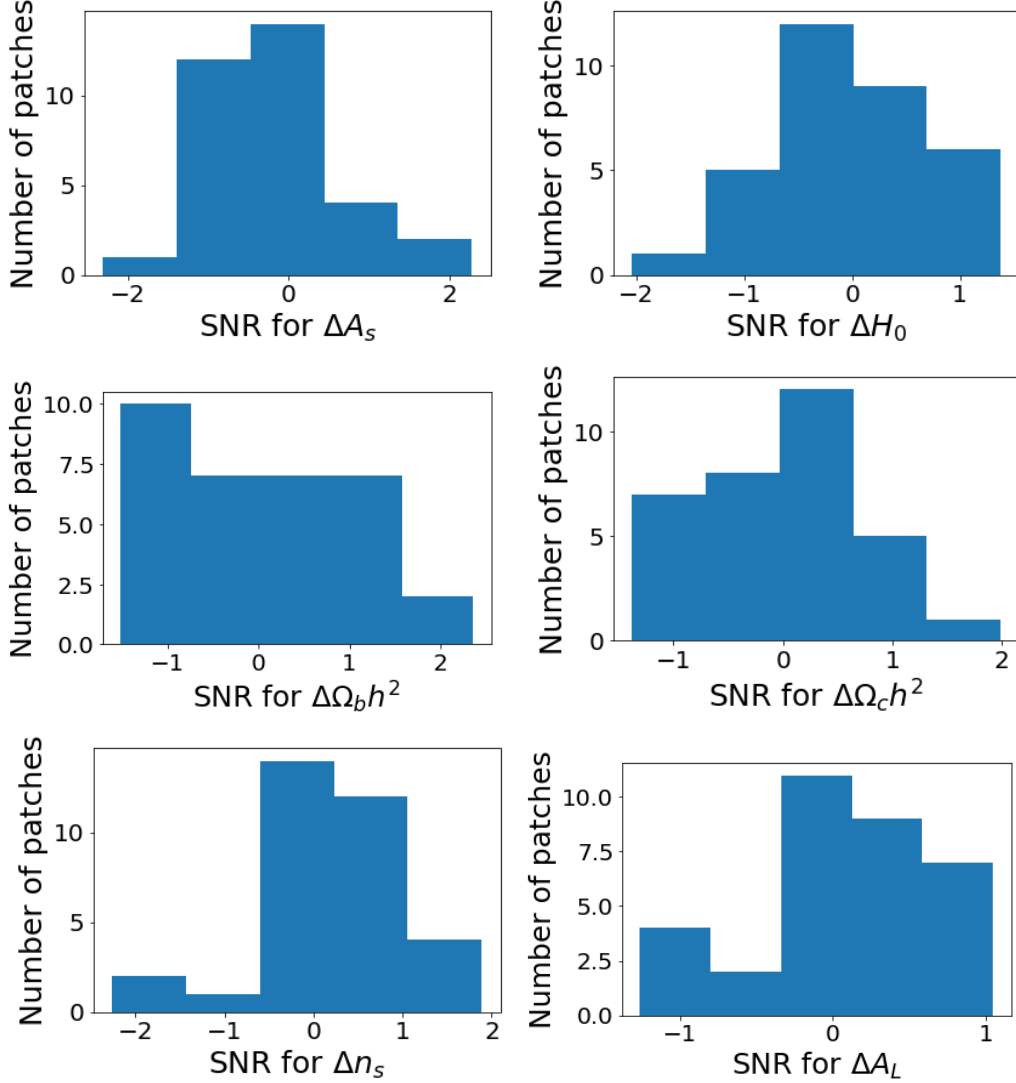


Figure 6: The distribution of SNR for cosmological parameters for different patches from Planck SMICA HM1 \times HM2. This is the case with bin width $\Delta l = 20$ used in the Master algorithm and CMB multipole range $[20, 1300]$. The distribution does not include the patches near the galactic plane having $f_{sky} \leq 0.017$.

3.3 Comparison of Planck SMICA results with CMB simulations

To scrutinize this in detail and evaluate the statistical significance of the parameter variations we saw in the SMICA map, we applied our method to 100 simulated temperature maps. The $\chi(\hat{n})$ values from 100 simulations (denoted by $\chi_s(\hat{n})$) for each patch are listed and are arranged in an ascending order, which can be named as $\mathcal{L}(\hat{n})$. Then the elements in the list $\mathcal{L}(\hat{n})$ are grouped in sets of ten and each set is indexed with a *group index*

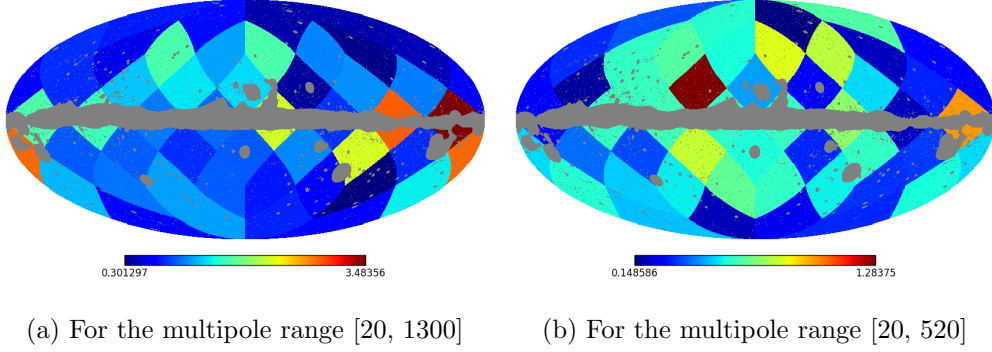


Figure 7: χ map for parameters (as expressed in Eq. (3.2)) for HM1 \times HM2 SMICA CMB sky with bin width of $\Delta l = 20$ used in the Master algorithm.

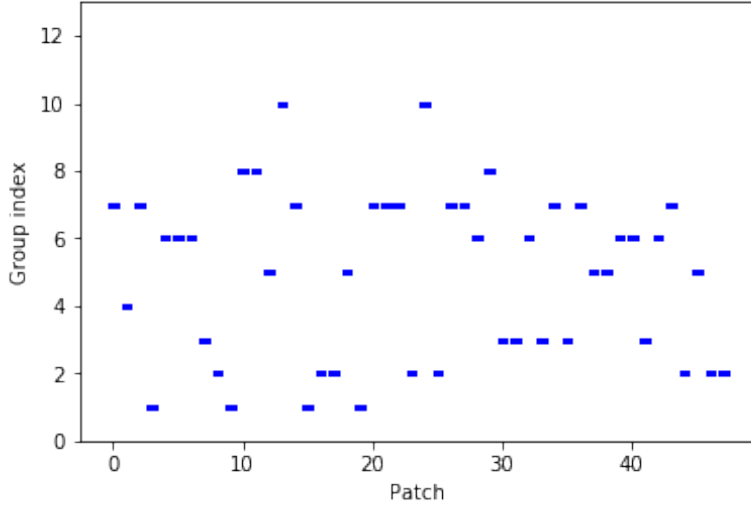
whose value varies from one to ten. For any particular patch centered in the direction \hat{n}_p , having the smallest $\chi_s(\hat{n}_p)$ value is the first element of the list \mathcal{L}^p and hence carries the *group index* = 1. Whereas the largest $\chi_s(\hat{n}_p)$ value is the last element of the list \mathcal{L}^p and carries the *group index* = 10.

The value of $\chi(\hat{n})$ from Planck SMICA map (denoted by $\chi_d(\hat{n})$) can be compared with the ordered list $\mathcal{L}(\hat{n})$ for every sky patches and we can obtain the *group index* which is associated with the value of χ_d . In this method of classification, the value of *group index* signifies the rank of the $\chi_d(\hat{n})$ value with respect to $\chi_s(\hat{n})$. For example, if χ_d value for a particular patch is having a *group index* = j , then there are at-least $10 \times (10 - j)$ simulations having χ_s value which are more than χ_d for that patch. If the value of χ_d is smaller (or greater) than the lowest (or highest) value of the list \mathcal{L} , then we show it by the down (or up) arrow.

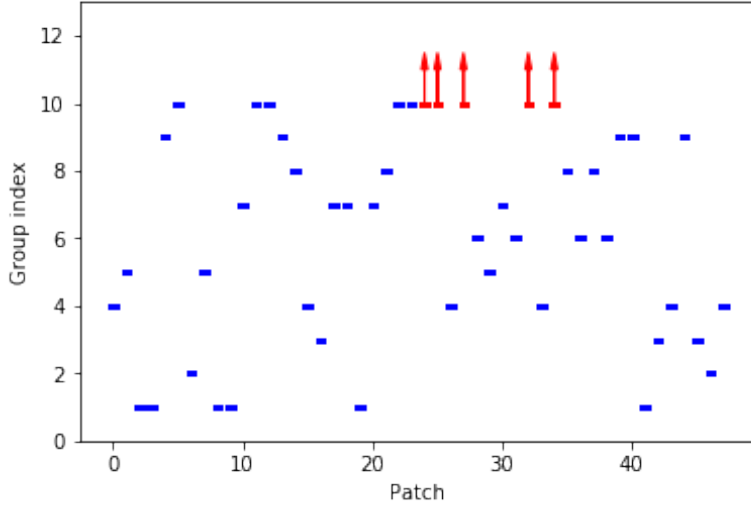
Using this prescription, we obtain the *group index* for all the sky patches and depict them in Fig. 8a and Fig. 8b for $l_{max} = 520$ and $l_{max} = 1300$ respectively. Fig. 8a shows that for all the patches with $l_{max} = 520$, Planck SMICA map is consistent with the values obtained from the simulations and none of the deviations in the cosmological parameters are significant. However, for $l_{max} = 1300$ depicted in Fig. 8b, a few patches near the galactic plane show higher deviations and do not match with the values of χ_s obtained from 100 simulations. These five patches are indicated by red arrows in Fig. 8b and can also be identified from the χ map in Fig. 7. All other patches are consistent with the statistically isotropic simulations and do not show any significant departures.

4 Conclusions

We described a fast algorithm to estimate the local variation of cosmological parameters from their fiducial value. In this method, we implement a local, optimal, quadratic filter that projects the data onto fields whose variances contain the cosmological parameter information. The full algorithm is described in Sec. 2. The advantage of this method is that it does not require costly MCMC analysis to obtain the deviations in the cosmologi-



(a) For the multipole range $[20, 520]$



(b) For the multipole range $[20, 1300]$

Figure 8: The *group index* of χ_p values from the Planck SMICA map are indicated for each sky patches for bin width $\Delta l = 20$ for (a) $l_{max} = 520$ and (b) $l_{max} = 1300$. The red arrows in the plot indicate the patches for which the values of χ_p is larger than the values observed in the simulations. All the patches except for five that intersect the galactic plane (colored yellow to red in Fig. 7) are consistent with the best-fit Planck parameters.

cal parameters. This makes the algorithm very useful to apply to any large data set. We implement it on the Planck SMICA-2015 temperature map to obtain the direction dependence of the six standard cosmological parameters ($A_s, n_s, O_b h^2, O_c h^2, H_0, A_L$). The

parameters maps are shown in Fig. 4 and Fig. 5 for two different choices of power spectrum binning $\Delta l = 50$ and $\Delta l = 20$ respectively. The maximum variation is evident in $\Omega_b h^2$ at approximately 2σ in two patches. In particular, parameters like H_0 , which shows some discrepancy compared to other data sets, and A_L which shows some tension with the expected value from standard model, do not show significant directional dependence. Our estimate shows that both these parameters are within the 2σ variation for all the patches. We find that A_L shows the least variations between patches in comparison to all other parameters. We compare our results with simulated uncontaminated CMB maps to get a better understanding of our SMICA results. We mask the simulated maps with the SMICA mask as shown in Fig. 3. Our simulation results indicate that the cosmological parameters based on the Planck SMICA-2015 temperature map do not exhibit higher variation than what is to be expected based on statistical fluctuations except in some patches on the galactic plane that are not used in the reference Planck analysis. On a χ map for SMICA (Fig. 7) for the range of multipoles $[20, 1300]$, we see that the parameter values in a few patches in the galactic plane exhibit a higher departure than our 100 simulations. But the patches at high galactic latitudes do not show any strong deviation in comparison to statistically isotropic simulations.

While the main motivation of our work was to provide a tool for checking for parameter variations that might visually correlate with known sources of systematics (from the Galaxy or more locally) our method can of course be used to explore a possible breaking of statistical isotropy. If a suggestive pattern were seen, it might motivate an in-depth analysis with a inference that is optimised for a particular physics model of isotropy breaking. We find no obvious indications of systematic parameter variations in the Planck SMICA map. A cross-correlation between the cosmological parameter map obtained from Planck SMICA-2015 and the results from the supernovae data by previous studies [20–22] can be useful to scrutinize any common direction dependence in the two different data sets.

In summary, we present an efficient algorithm to check for any directional dependence of the cosmological parameters. Due to the computational efficiency of our method, it can be used for large data sets, to check for the effects of contaminations from unknown systematics on the estimated cosmological parameters. This method is applicable not only to CMB data set but adapts to other data sets, such as galaxy surveys, weak-lensing shear measurements, and 21 cm data with minimal effort.

Future observational campaigns promise to deliver robust measurements of cosmological parameters despite challenging foreground and noise contaminations. The methods we present in this paper add an efficient diagnostic tool to assess how these final science products are affected by potential instrumental or astrophysical systematics.

Acknowledgements This work has been done within the Labex ILP (reference ANR-10-LABX-63) part of the Idex SUPER, and received financial state aid managed by the Agence Nationale de la Recherche, as part of the programme Investissements d’avenir under the reference ANR-11-IDEX-0004-02. This work is supported by the Simons Foundation. The author acknowledges the use of CAMB, HEALPix and MASTER

algorithm in this analysis.

References

- [1] A. A. Penzias and R. W. Wilson. A Measurement of Excess Antenna Temperature at 4080 Mc/s. *ApJ*, 142:419–421, July 1965. [\[DOI\]](#), [\[ADS\]](#).
- [2] D. J. Fixsen, E. S. Cheng, J. M. Gales, J. C. Mather, R. A. Shafer, and E. L. Wright. The Cosmic Microwave Background Spectrum from the Full COBE FIRAS Data Set. *ApJ*, 473:576, 1996. [\[DOI\]](#), [\[ADS\]](#).
- [3] D. J. Fixsen, G. Hinshaw, C. L. Bennett, and J. C. Mather. The Spectrum of the Cosmic Microwave Background Anisotropy from the Combined COBE FIRAS and DMR Observations. *ApJ*, 486:623–628, September 1997. [arXiv:astro-ph/9704176](#), [\[DOI\]](#), [\[ADS\]](#).
- [4] D. J. Fixsen and J. C. Mather. The Spectral Results of the Far-Infrared Absolute Spectrophotometer Instrument on COBE. *ApJ*, 581:817–822, 2002. [\[DOI\]](#), [\[ADS\]](#).
- [5] E. L. Wright, C. L. Bennett, K. Gorski, G. Hinshaw, and G. F. Smoot. Angular Power Spectrum of the Cosmic Microwave Background Anisotropy seen by the COBE DMR. *ApJL*, 464:L21, 1996. [\[DOI\]](#), [\[ADS\]](#).
- [6] C. L. Bennett, D. Larson, J. L. Weiland, N. Jarosik, G. Hinshaw, N. Odegard, K. M. Smith, R. S. Hill, B. Gold, M. Halpern, E. Komatsu, M. R. Nolta, L. Page, D. N. Spergel, E. Wollack, J. Dunkley, A. Kogut, M. Limon, S. S. Meyer, G. S. Tucker, and E. L. Wright. Nine-year Wilkinson Microwave Anisotropy Probe (WMAP) Observations: Final Maps and Results. *ApJS*, 208:20, October 2013. [arXiv:1212.5225](#), [\[DOI\]](#), [\[ADS\]](#).
- [7] Planck Collaboration, R. Adam, P. A. R. Ade, N. Aghanim, Y. Akrami, M. I. R. Alves, F. Argüeso, M. Arnaud, F. Arroja, M. Ashdown, and et al. Planck 2015 results. I. Overview of products and scientific results. *A&A*, 594:A1, September 2016. [arXiv:1502.01582](#), [\[DOI\]](#), [\[ADS\]](#).
- [8] D. Hanson, S. Hoover, A. Crites, P. A. R. Ade, K. A. Aird, J. E. Austermann, J. A. Beall, A. N. Bender, B. A. Benson, L. E. Bleem, J. J. Bock, J. E. Carlstrom, C. L. Chang, H. C. Chiang, H.-M. Cho, A. Conley, T. M. Crawford, T. de Haan, M. A. Dobbs, W. Everett, J. Gallicchio, J. Gao, E. M. George, N. W. Halverson, N. Harrington, J. W. Henning, G. C. Hilton, G. P. Holder, W. L. Holzapfel, J. D. Hrubes, N. Huang, J. Hubmayr, K. D. Irwin, R. Keisler, L. Knox, A. T. Lee, E. Leitch, D. Li, C. Liang, D. Luong-Van, G. Marsden, J. J. McMahon, J. Mehl, S. S. Meyer, L. Mocanu, T. E. Montroy, T. Natoli, J. P. Nibarger, V. Novosad, S. Padin, C. Pryke, C. L. Reichardt, J. E. Ruhl, B. R. Saliwanchik, J. T. Sayre, K. K. Schaffer, B. Schulz, G. Smecher, A. A. Stark, K. T. Story, C. Tucker, K. Vanderlinde, J. D. Vieira, M. P. Viero, G. Wang, V. Yefremenko, O. Zahn, and M. Zemcov. Detection of B-Mode Polarization in the Cosmic Microwave Background with Data from the South Pole Telescope. *Physical Review Letters*, 111(14):141301, October 2013. [arXiv:1307.5830](#), [\[DOI\]](#), [\[ADS\]](#).
- [9] S. Das, B. D. Sherwin, P. Aguirre, J. W. Appel, J. R. Bond, C. S. Carvalho, M. J. Devlin, J. Dunkley, R. Dünner, T. Essinger-Hileman, J. W. Fowler, A. Hajian, M. Halpern, M. Hasselfield, A. D. Hincks, R. Hlozek, K. M. Huffenberger, J. P. Hughes, K. D. Irwin, J. Klein, A. Kosowsky, R. H. Lupton, T. A. Marriage, D. Marsden, F. Menanteau, K. Moodley, M. D. Niemack, M. R. Nolta, L. A. Page, L. Parker, E. D. Reese, B. L.

- Schmitt, N. Sehgal, J. Sievers, D. N. Spergel, S. T. Staggs, D. S. Swetz, E. R. Switzer, R. Thornton, K. Visnjic, and E. Wollack. Detection of the Power Spectrum of Cosmic Microwave Background Lensing by the Atacama Cosmology Telescope. *Physical Review Letters*, 107(2):021301, July 2011. [arXiv:1103.2124](#), [DOI], [ADS].
- [10] BICEP2 Collaboration, Keck Array Collaboration, P. A. R. Ade, Z. Ahmed, R. W. Aikin, K. D. Alexander, D. Barkats, S. J. Benton, C. A. Bischoff, J. J. Bock, R. Bowens-Rubin, J. A. Brevik, I. Buder, E. Bullock, V. Buza, J. Connors, B. P. Crill, L. Duband, C. Dvorkin, J. P. Filippini, S. Fliescher, J. Grayson, M. Halpern, S. Harrison, S. R. Hildebrandt, G. C. Hilton, H. Hui, K. D. Irwin, J. Kang, K. S. Karkare, E. Karpel, J. P. Kaufman, B. G. Keating, S. Kefeli, S. A. Kernasovskiy, J. M. Kovac, C. L. Kuo, E. M. Leitch, M. Lueker, K. G. Megerian, T. Namikawa, C. B. Netterfield, H. T. Nguyen, R. O’Brien, R. W. Ogburn, IV, A. Orlando, C. Pryke, S. Richter, R. Schwarz, C. D. Sheehy, Z. K. Staniszewski, B. Steinbach, R. V. Sudiwala, G. P. Teply, K. L. Thompson, J. E. Tolan, C. Tucker, A. D. Turner, A. G. Vieregge, A. C. Weber, D. V. Wiebe, J. Willmert, C. L. Wong, W. L. K. Wu, and K. W. Yoon. BICEP2/Keck Array VIII: Measurement of Gravitational Lensing from Large-scale B-mode Polarization. *ApJ*, 833:228, December 2016. [arXiv:1606.01968](#), [DOI], [ADS].
- [11] P. A. R. Ade, Y. Akiba, A. E. Anthony, K. Arnold, M. Atlas, D. Barron, D. Boettger, J. Borrill, S. Chapman, Y. Chinone, M. Dobbs, T. Elleflot, J. Errard, G. Fabbian, C. Feng, D. Flanagan, A. Gilbert, W. Grainger, N. W. Halverson, M. Hasegawa, K. Hattori, M. Hazumi, W. L. Holzapfel, Y. Hori, J. Howard, P. Hyland, Y. Inoue, G. C. Jaehnig, A. Jaffe, B. Keating, Z. Kermish, R. Keskitalo, T. Kisner, M. Le Jeune, A. T. Lee, E. Linder, E. M. Leitch, M. Lungu, F. Matsuda, T. Matsumura, X. Meng, N. J. Miller, H. Morii, S. Moyerman, M. J. Myers, M. Navaroli, H. Nishino, H. Paar, J. Peloton, E. Quealy, G. Rebeiz, C. L. Reichardt, P. L. Richards, C. Ross, I. Schanning, D. E. Schenck, B. Sherwin, A. Shimizu, C. Shimmin, M. Shimon, P. Siritanasak, G. Smecher, H. Spieler, N. Stebor, B. Steinbach, R. Stompor, A. Suzuki, S. Takakura, T. Tomaru, B. Wilson, A. Yadav, O. Zahn, and Polarbear Collaboration. Measurement of the Cosmic Microwave Background Polarization Lensing Power Spectrum with the POLARBEAR Experiment. *Physical Review Letters*, 113(2):021301, July 2014. [arXiv:1312.6646](#), [DOI], [ADS].
- [12] C. J. MacTavish, P. A. R. Ade, J. J. Bock, J. R. Bond, J. Borrill, A. Boscaleri, P. Cabella, C. R. Contaldi, B. P. Crill, P. de Bernardis, G. De Gasperis, A. de Oliveira-Costa, G. De Troia, G. di Stefano, E. Hivon, A. H. Jaffe, W. C. Jones, T. S. Kisner, A. E. Lange, A. M. Lewis, S. Masi, P. D. Mauskopf, A. Melchiorri, T. E. Montroy, P. Natoli, C. B. Netterfield, E. Pascale, F. Piacentini, D. Pogosyan, G. Polenta, S. Prunet, S. Ricciardi, G. Romeo, J. E. Ruhl, P. Santini, M. Tegmark, M. Veneziani, and N. Vittorio. Cosmological Parameters from the 2003 Flight of BOOMERANG. *ApJ*, 647:799–812, August 2006. [arXiv:astro-ph/0507503](#), [DOI], [ADS].
- [13] R. Stompor, S. Hanany, M. E. Abroe, J. Borrill, P. G. Ferreira, A. H. Jaffe, B. Johnson, A. T. Lee, B. Rabii, P. L. Richards, G. Smoot, C. Winant, and J. H. P. Wu. The MAXIMA Experiment: Latest Results and Consistency Tests. *ArXiv Astrophysics e-prints*, September 2003. [arXiv:astro-ph/0309409](#), [ADS].
- [14] Y. Mellier. Euclid: Mapping the Geometry of the Dark Universe. In *Science from the Next Generation Imaging and Spectroscopic Surveys*, page 3, October 2012. [ADS].
- [15] LSST Science Collaboration, P. A. Abell, J. Allison, S. F. Anderson, J. R. Andrew,

- J. R. P. Angel, L. Armus, D. Arnett, S. J. Asztalos, T. S. Axelrod, and et al. LSST Science Book, Version 2.0. *ArXiv e-prints*, December 2009. [arXiv:0912.0201](#), [ADS].
- [16] Chris L. Carilli and S. Rawlings. Science with the Square Kilometer Array: Motivation, key science projects, standards and assumptions. *New Astron. Rev.*, 48:979, 2004. [arXiv:astro-ph/0409274](#), [DOI].
- [17] A. Kogut, D. J. Fixsen, D. T. Chuss, J. Dotson, E. Dwek, M. Halpern, G. F. Hinshaw, S. M. Meyer, S. H. Moseley, M. D. Seiffert, D. N. Spergel, and E. J. Wollack. The Primordial Inflation Explorer (PIXIE): a nulling polarimeter for cosmic microwave background observations. *JCAP*, 7:25, 2011. [arXiv:1105.2044](#), [DOI], [ADS].
- [18] T. Matsumura et al. Mission design of LiteBIRD. 2013. [J. Low. Temp. Phys.176,733(2014)]. [arXiv:1311.2847](#), [DOI].
- [19] Antony Lewis and Sarah Bridle. Cosmological parameters from CMB and other data: A Monte Carlo approach. *Phys. Rev.*, D66:103511, 2002. [arXiv:astro-ph/0205436](#), [DOI].
- [20] Behnam Javanmardi, Cristiano Porciani, Pavel Kroupa, and Jan Pflamm-Altenburg. Probing the isotropy of cosmic acceleration traced by Type Ia supernovae. *Astrophys. J.*, 810(1):47, 2015. [arXiv:1507.07560](#), [DOI].
- [21] C. Sofia Carvalho and Katrine Marques. Angular distribution of cosmological parameters as a probe of space-time inhomogeneities. *Astron. Astrophys.*, 592:A102, 2016. [arXiv:1512.07869](#), [DOI].
- [22] C. Sofia Carvalho and Spyros Basilakos. Angular distribution of cosmological parameters as a probe of inhomogeneities: a kinematic parametrisation. *Astron. Astrophys.*, 592:A152, 2016. [arXiv:1603.07519](#), [DOI].
- [23] Rong-Gen Cai and Zhong-Liang Tuo. Direction Dependence of the Deceleration Parameter. *JCAP*, 1202:004, 2012. [arXiv:1109.0941](#), [DOI].
- [24] M. Axelsson, Y. Fantaye, F. K. Hansen, A. J. Banday, H. K. Eriksen, and K. M. Gorski. Directional Dependence of Λ CDM Cosmological Parameters. *ApJL*, 773:L3, August 2013. [arXiv:1303.5371](#), [DOI], [ADS].
- [25] S. Mukherjee, P. K. Aluri, S. Das, S. Shaikh, and T. Souradeep. Direction dependence of cosmological parameters due to cosmic hemispherical asymmetry. *JCAP*, 6:042, June 2016. [arXiv:1510.00154](#), [DOI], [ADS].
- [26] D. K. Hazra and A. Shafieloo. Search for a direction in the forest of Lyman- α . *JCAP*, 11:012, November 2015. [arXiv:1506.03926](#), [DOI], [ADS].
- [27] K. Tomita. Anisotropy of the Hubble Constant in a Cosmological Model with a Local Void on Scales of ~ 200 Mpc. *Progress of Theoretical Physics*, 105:419–427, March 2001. [arXiv:astro-ph/0005031](#), [DOI], [ADS].
- [28] M.L. McClure and C.C. Dyer. Anisotropy in the hubble constant as observed in the {HST} extragalactic distance scale key project results. *New Astronomy*, 12(7):533 – 543, 2007. URL: <http://www.sciencedirect.com/science/article/pii/S1384107607000231>, [DOI].
- [29] Antonio Enea Romano and Sergio Andr  s Vallejo. Directional dependence of the local estimation of H_0 and the nonperturbative effects of primordial curvature perturbations. *Europhys. Lett.*, 109(3):39002, 2015. [arXiv:1403.2034](#), [DOI].

- [30] Alan Zablacki and Scott Dodelson. Extreme data compression for the cmb. *Phys. Rev. D*, 93:083525, Apr 2016. URL: <https://link.aps.org/doi/10.1103/PhysRevD.93.083525>, [DOI].
- [31] Suvodip Mukherjee and Tarun Souradeep. Litmus Test for Cosmic Hemispherical Asymmetry in the Cosmic Microwave Background B-mode polarization. *Phys. Rev. Lett.*, 116(22):221301, 2016. [arXiv:1509.06736](https://arxiv.org/abs/1509.06736), [DOI].
- [32] N. J. Cornish, D. N. Spergel, and G. D. Starkman. Circles in the sky: finding topology with the microwave background radiation. *Classical and Quantum Gravity*, 15:2657–2670, September 1998. [arXiv:gr-qc/9602039](https://arxiv.org/abs/gr-qc/9602039), [DOI], [ADS].
- [33] A. Hajian. Are there Echoes from the Pre-big-bang Universe? A Search for Low-variance Circles in the Cosmic Microwave Background Sky. *ApJ*, 740:52, October 2011. [arXiv:1012.1656](https://arxiv.org/abs/1012.1656), [DOI], [ADS].
- [34] E. D. Kovetz, A. Ben-David, and N. Itzhaki. Giant Rings in the Cosmic Microwave Background Sky. *ApJ*, 724:374–378, November 2010. [arXiv:1005.3923](https://arxiv.org/abs/1005.3923), [DOI], [ADS].
- [35] A. Moss, D. Scott, and J. P. Zibin. No evidence for anomalously low variance circles on the sky. *JCAP*, 4:033, April 2011. [arXiv:1012.1305](https://arxiv.org/abs/1012.1305), [DOI], [ADS].
- [36] P. Bielewicz, B. D. Wandelt, and A. J. Banday. A search for concentric rings with unusual variance in the 7-year WMAP temperature maps using a fast convolution approach. *MNRAS*, 429:1376–1385, February 2013. [arXiv:1207.6905](https://arxiv.org/abs/1207.6905), [DOI], [ADS].
- [37] A. Fialkov, N. Itzhaki, and E. D. Kovetz. Cosmological imprints of pre-inflationary particles. *JCAP*, 2:004, February 2010. [arXiv:0911.2100](https://arxiv.org/abs/0911.2100), [DOI], [ADS].
- [38] S. M. Feeney, M. C. Johnson, D. J. Mortlock, and H. V. Peiris. First observational tests of eternal inflation: Analysis methods and WMAP 7-year results. *Phys.Rev.D*, 84(4):043507, August 2011. [arXiv:1012.3667](https://arxiv.org/abs/1012.3667), [DOI], [ADS].
- [39] Max Tegmark. How to measure CMB power spectra without losing information. *Phys. Rev.*, D55:5895–5907, 1997. [arXiv:astro-ph/9611174](https://arxiv.org/abs/astro-ph/9611174), [DOI].
- [40] J. R. Bond, Andrew H. Jaffe, and L. Knox. Estimating the power spectrum of the cosmic microwave background. *Phys. Rev.*, D57:2117–2137, 1998. [arXiv:astro-ph/9708203](https://arxiv.org/abs/astro-ph/9708203), [DOI].
- [41] Siang Peng Oh, David N. Spergel, and Gary Hinshaw. An Efficient technique to determine the power spectrum from cosmic microwave background sky maps. *Astrophys. J.*, 510:551, 1999. [arXiv:astro-ph/9805339](https://arxiv.org/abs/astro-ph/9805339), [DOI].
- [42] Benjamin D. Wandelt, David L. Larson, and Arun Lakshminarayanan. Global, exact cosmic microwave background data analysis using Gibbs sampling. *Phys. Rev.*, D70:083511, 2004. [arXiv:astro-ph/0310080](https://arxiv.org/abs/astro-ph/0310080), [DOI].
- [43] Franz Elsner and Benjamin D. Wandelt. Fast calculation of the Fisher matrix for Cosmic Microwave Background experiments. *Astron. Astrophys.*, 540:L6, 2012. [arXiv:1202.4898](https://arxiv.org/abs/1202.4898), [DOI].
- [44] G. Hinshaw et al. First year Wilkinson Microwave Anisotropy Probe (WMAP) observations: Data processing methods and systematic errors limits. *Astrophys. J. Suppl.*, 148:63, 2003. [arXiv:astro-ph/0302222](https://arxiv.org/abs/astro-ph/0302222), [DOI].
- [45] J. Dunkley et al. Five-Year Wilkinson Microwave Anisotropy Probe (WMAP)

- Observations: Likelihoods and Parameters from the WMAP data. *Astrophys. J. Suppl.*, 180:306–329, 2009. [arXiv:0803.0586](#), [\[DOI\]](#).
- [46] Franz Elsner and Benjamin D. Wandelt. Likelihood, Fisher information, and systematics of cosmic microwave background experiments. *Astron. Astrophys.*, 542:A60, 2012. [arXiv:1205.0810](#), [\[DOI\]](#).
 - [47] Max Tegmark. How to make maps from CMB data without losing information. *Astrophys. J.*, 480:L87–L90, 1997. [arXiv:astro-ph/9611130](#), [\[DOI\]](#).
 - [48] Christopher M. Hirata, Nikhil Padmanabhan, Uros Seljak, David Schlegel, and Jonathan Brinkmann. Cross-correlation of CMB with large-scale structure: Weak gravitational lensing. *Phys. Rev.*, D70:103501, 2004. [arXiv:astro-ph/0406004](#), [\[DOI\]](#).
 - [49] Kendrick M. Smith, Oliver Zahn, and Olivier Dore. Detection of Gravitational Lensing in the Cosmic Microwave Background. *Phys. Rev.*, D76:043510, 2007. [arXiv:0705.3980](#), [\[DOI\]](#).
 - [50] Franz Elsner and Benjamin D. Wandelt. Efficient Wiener filtering without preconditioning. *Astron. Astrophys.*, 549:A111, 2013. [arXiv:1210.4931](#), [\[DOI\]](#).
 - [51] Emory F. Bunn and Benjamin Wandelt. Pure E and B polarization maps via Wiener filtering. 2016. [arXiv:1610.03345](#).
 - [52] Doogesh Kodi Ramanah, Guilhem Lavaux, and Benjamin D. Wandelt. Wiener filter reloaded: fast signal reconstruction without preconditioning. *Mon. Not. Roy. Astron. Soc.*, 468(2):1782–1793, 2017. [arXiv:1702.08852](#), [\[DOI\]](#).
 - [53] S. Gupta and A. F. Heavens. Fast parameter estimation from the cosmic microwave background power spectrum. *MNRAS*, 334:167–172, July 2002. [arXiv:astro-ph/0108315](#), [\[DOI\]](#), [\[ADS\]](#).
 - [54] Planck 2015 results: SMICA Temperature Map.
 - [55] M. G. Hauser and P. J. E. Peebles. Statistical Analysis of Catalogs of Extragalactic Objects. II. the Abell Catalog of Rich Clusters. *ApJ*, 185:757–786, November 1973. [\[DOI\]](#), [\[ADS\]](#).
 - [56] Benjamin D. Wandelt, Eric Hivon, and Krzysztof M. Gorski. The pseudo- c_l method: cosmic microwave background anisotropy power spectrum statistics for high precision cosmology. *Phys. Rev.*, D64:083003, 2001. [arXiv:astro-ph/0008111](#), [\[DOI\]](#).
 - [57] E. Hivon, K. M. Gorski, C. B. Netterfield, B. P. Crill, S. Prunet, and F. Hansen. Master of the cosmic microwave background anisotropy power spectrum: a fast method for statistical analysis of large and complex cosmic microwave background data sets. *Astrophys. J.*, 567:2, 2002. [arXiv:astro-ph/0105302](#), [\[DOI\]](#).
 - [58] Max Tegmark, Andy Taylor, and Alan Heavens. Karhunen-Loeve eigenvalue problems in cosmology: How should we tackle large data sets? *Astrophys. J.*, 480:22, 1997. [arXiv:astro-ph/9603021](#), [\[DOI\]](#).
 - [59] K. M. Gorski, Eric Hivon, A. J. Banday, B. D. Wandelt, F. K. Hansen, M. Reinecke, and M. Bartelman. HEALPix - A Framework for high resolution discretization, and fast analysis of data distributed on the sphere. *Astrophys. J.*, 622:759–771, 2005. [arXiv:astro-ph/0409513](#), [\[DOI\]](#).
 - [60] P. A. R. Ade et al. Planck 2015 results. XIII. Cosmological parameters. *Astron. Astrophys.*, 594:A13, 2016. [arXiv:1502.01589](#), [\[DOI\]](#).

- [61] Antony Lewis, Anthony Challinor, and Anthony Lasenby. Efficient computation of CMB anisotropies in closed FRW models. *Astrophys. J.*, 538:473–476, 2000. [arXiv:astro-ph/9911177](#), [DOI].
- [62] N. Aghanim et al. Planck intermediate results. XLIX. Parity-violation constraints from polarization data. *Astron. Astrophys.*, 596:A110, 2016. [arXiv:1605.08633](#), [DOI].